IOPscience iopscience.iop.org

Home Search Collections Journals About Contact us My IOPscience

Numerical simulation of the steady state photoconductivity in hydrogenated amorphous silicon including localized state electron hopping

This article has been downloaded from IOPscience. Please scroll down to see the full text article.

2006 J. Phys.: Condens. Matter 18 3721

(http://iopscience.iop.org/0953-8984/18/15/017)

View the table of contents for this issue, or go to the journal homepage for more

Download details:
IP Address: 129.252.86.83
The article was downloaded on 28/05/2010 at 10:04

Please note that terms and conditions apply.

INSTITUTE OF PHYSICS PUBLISHING JOURNAL OF PHYSICS: CONDENSED MATTER

J. Phys.: Condens. Matter **18** (2006) 3721–3734 doi:10.1088/0953-8984/18/15/017

Numerical simulation of the steady state photoconductivity in hydrogenated amorphous silicon including localized state electron hopping

A Merazga[1], **S Tobbeche**[2], **C Main**[3], **A Al-Shahrani**[1] **and S Reynolds**[4]

[1] Department of Physics, Faculty of Science, King Khalid University, PO Box 9004, Abha, Saudi Arabia
[2] Department of Electronics, Faculty of Science and Engineering, University Mohammed Khider, PO Box 154, Biskra 07000, Algeria
[3] Division of Electronic Engineering and Physics, Dundee University, Dundee DD1 4HN, UK
[4] Institute of Photovoltaics, Forschungszentrum Jülich, Germany

E-mail: aamerazga@kku.edu.sa

Received 21 December 2005, in final form 27 February 2006
Published 30 March 2006
Online at stacks.iop.org/JPhysCM/18/3721

Abstract
Numerical simulation of the steady state photoconductivity in hydrogenated amorphous silicon over a wide temperature range (25–500 K) is extended, to include previously neglected carrier transitions between localized states. In addition to free carrier capture (emission) transitions into (from) localized states, we include the process of electron hopping in conduction band tail states. Exponential distributions are assumed for both conduction and valence band tail states, while the dangling bond defect distribution is calculated in accordance with the defect pool model. Localized to extended state transitions follow the Simmons and Taylor statistics, and localized to localized state transitions involve electron hopping between nearest neighbour sites. Comparison with simulations in the absence of electron hopping reveals a smooth transition around 110 K, between regions of (high temperature) extended state conduction and (low temperature) hopping conduction. A hopping transport energy level is identified as the peak of the energy distribution of the hopping photocarriers, and shows a temperature dependence in agreement with existing theoretical work.

1. Introduction

Typical measurements of steady state photoconductivity (SSPC) in hydrogenated amorphous silicon (a-Si:H) as a function of temperature and doping are shown in figure 1 [1], covering a wide temperature range and showing all the SSPC features [1, 2]. In the undoped case, for instance, four regions can be distinguished: region (I) at very low temperatures ($T < 50$ K), where the SSPC is independent of temperature, region (II) at intermediate temperatures ($50\text{ K} < T < 150$ K), where the SSPC rises with increasing temperature by several orders of

0953-8984/06/153721+14$30.00 © 2006 IOP Publishing Ltd Printed in the UK

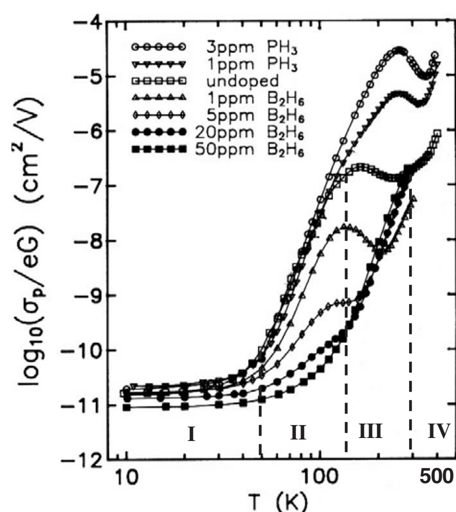

Figure 1. Temperature dependence of the normalized SSPC (σ_{ph}/eG) in logarithmic scale for undoped, p-type and n-type a-Si:H. The dopant concentration in the plasma gas is indicated. The samples were exposed for 30 min to 70 mW cm^{-2}, $h\nu = 2$ eV, light prior to measurement [1]. The vertical lines separate, in the undoped case, the four temperature regions described in the text. Note that in [1], the authors used the symbol σ_p for the SSPC.

magnitude, showing a well defined activation energy, region (III) at relatively high temperatures, where the SSPC saturates and possibly decreases with increasing temperature, showing a thermal quenching feature, and finally region (IV) at high temperatures ($T > 300$ K), where the SSPC increases rapidly with temperature. In region (I), the SSPC is also a linear function of the excitation intensity G in such a way that the normalized photoconductivity $\sigma_{ph}/(eG)$, where e is the electron charge, is equal to about 2×10^{-11} cm^2 V^{-1}.

Most of the early models developed to explain observed features of the SSPC in a-Si:H were concerned with temperature ranges above 100 K and, therefore, have ignored the localized–localized state carrier hopping [3–6]. They use the Simmons and Taylor statistics for carrier occupancies [7], but differ in the density of states (DOS) distribution and the recombination mechanism. Vaillant *et al* [3] proposed discrete dangling bond (DB) levels and exponential band tails (BTs) to simulate the temperature dependence of SSPC. Their model predicts that the contribution to recombination via DB states starts dominating at relatively high temperatures. The agreement with the experiment is excellent above 150 K, while below this temperature the model overestimates the experimental SSPC. Other models, using exponential BT and a single level of DB recombination centres, have considered BT-to-DB recombination [8] and BT-to-BT tunnelling recombination [9, 10] to provide an explanation of some particular SSPC features observed within a limited temperature ranges. For example, the model of Zhou *et al* [9] could account for the variation of SSPC in region (II), but the magnitude of the predicted SSPC is larger than the measured one.

It was early concluded by many groups that the SSPC in the low temperature region is due to electron hopping (EH) in the conduction band tail (CBT) [11–16]. Shklovskii *et al* [14] developed a theory to explain the photoconductivity in this temperature range, in which geminate recombination and electron hopping through localized states were considered. Baranovskii *et al* [16] have also developed a theory for the low and intermediate temperature regions (I) and (II), whereby they explain the increase of the SSPC with temperature in terms

of a transport energy level E_t at which the electron hopping contribution is a maximum. This coincided with the transport energy E_t defined earlier by Monroe [15], considering the transient photoresponse at the long time limit. With increasing temperature, E_t moves upward into more shallow localized states and the upward hops of electrons to the vicinity of E_t determine the hopping transport.

The primary purpose of this work is to provide a numerical simulation for the temperature dependence of SSPC in a-Si:H, combining the two conduction mechanisms related to extended state diffusive transport and localized state hopping transport. We consider exponential conduction and valence band tails (VBTs) and use the defect pool model (DPM) for the DB defect density [17, 18]. The resulting density of states with three components of different state types (the VBT donor-like states, the CBT acceptor-like states and the DB defect states) is used to simulate the SSPC. We follow the numerical method applied by Main *et al* [19] to simulate multiple trapping and hopping transport in the transient photocurrent case. This method consists of dividing the energy gap into closely spaced energy levels and solving simultaneously coupled rate equations corresponding to each level, for all free and trapped carrier densities.

In contrast to previous simulation work which concentrates on limited ranges in the temperature variation of SSPC and neglects localized–localized state transitions, the present SSPC simulation is designed to cover low, intermediate and high temperature regions in a single model that couples localized–extended and localized–localized state carrier transitions. The SSPC features of figure 1 are successfully reproduced by the simulated SSPC. With decreasing temperature at moderate light intensity, the EH mechanism starts having a significant contribution at about 110 K, causing an increase of the SSPC activation energy in the intermediate temperature range (100–70 K). It then dominates the SSPC, leading to a constant SSPC below 50 K. Altering the doping smoothly from p-type through to n-type affects considerably the region of extended state conduction above 110 K by raising towards higher temperature. It has little effect on the intermediate activated region and practically no effect on the constant SSPC dominated by EH. These simulations show an overall agreement with experiment, and are interpreted in terms of doping induced changes in the DPM defect charges on the high temperature side, and the relative contribution of EH to SSPC on the low temperature side.

2. SSPC simulation

2.1. Density of states distribution

The DOS distribution includes exponential CBT and VBT:

$$g_c(E) = G_c \exp\left(\frac{E - E_c}{k_B T_c}\right) \qquad \text{and} \qquad g_v(E) = G_v \exp\left(\frac{E_v - E}{k_B T_v}\right). \tag{1}$$

Here k_B is the Boltzmann constant. Model values of $T_c = 300$ K, $T_v = 650$ K, $G_c = 5 \times 10^{22}$ cm^{-3} eV^{-1} and $G_v = 10^{21}$ cm^{-3} eV^{-1} were chosen, in agreement with the literature. The CBT and the VBT states are treated as acceptor- and donor-like states, respectively. For the DB states, we follow the DPM calculation [17, 18] leading to the DOS expression

$$D(E) = \xi \left(\frac{2}{f^0(E)}\right)^{\alpha} P\left(E + \frac{\sigma^2}{2E_{vo}}\right) \tag{2}$$

with

$$\xi = \left(\frac{G_v 2E_{vo}^2}{(2E_{vo} - k_B T^*)}\right)\left(\frac{H}{N_{SiSi}}\right)^{\frac{\alpha}{2}} \exp\left(\frac{-1}{2E_{vo}}\left(E_p - E_v - \frac{\sigma^2}{4E_{vo}}\right)\right),$$

Table 1. Parameters for the gap density of states.

E_g (eV)	1.9
G_v (cm^{-3} eV^{-1})	10^{21}
T_v (K)	650
σ (eV)	0.19
$E_c - E_p$ (eV)	0.63
E_{vo} (meV)	56
N_{SiSi} (cm^{-3})	2×10^{23}
H (cm^{-3})	5×10^{21}
U (eV)	0.2
T^* (K)	500
G_c (cm^{-3} eV^{-1})	5×10^{22}
T_c (K)	320

where $\alpha = k_B T^*/2E_{vo}$. $P(E)$ is the Gaussian shaped defect pool with σ and E_p respectively its width and peak position in the gap. $E_{vo} = k_B T_v$ is the width of the exponential VBT. H and N_{SiSi} are the total hydrogen and silicon concentrations, respectively. T^* is the equilibrium temperature (freeze-in temperature). The density of DB states with different charges, neutral state (or singly occupied) D^0, positively charged (or unoccupied) D^+ and negatively charged (or doubly occupied) D^-, are respectively given by

$$D^0(E) = D(E) f^0(E) \tag{3}$$

$$D^+(E) = D(E) f^+(E) \tag{4}$$

$$D^-(E) = D(E) f^-(E) \tag{5}$$

where the thermal equilibrium occupation functions f^+, f^0 and f^- [20], the probabilities for the DB state of being, respectively, unoccupied D^+, singly occupied D^0 and doubly occupied D^-, are

$$f^+(E) = 1 \Big/ \left[1 + 2\exp\left(\frac{E_F - E}{k_B T}\right) + \exp\left(\frac{2E_F - 2E - U}{k_B T}\right)\right] \tag{6}$$

$$f^0(E) = 2\exp\left(\frac{E_F - E}{k_B T}\right) f^+(E) \tag{7}$$

$$f^-(E) = \exp\left(\frac{2E_F - 2E - U}{k_B T}\right) f^+(E). \tag{8}$$

The Fermi level position E_F in the gap is determined by solving the charge neutrality condition involving all free and trapped charges, which is also satisfied in the steady state quasi-equilibrium. E_c and E_v are respectively the conduction and valence mobility edges and U is the correlation energy. The DOS parameters used in the DPM calculation are given in table 1. Figure 2 shows the DB density of states distribution, $D(E)$, for undoped and lightly doped n-type and p-type a-Si:H. The CBT $g_c(E)$ and VBT $g_v(E)$ are also shown. The arrows point to the dark Fermi level positions below E_c: 0.87 eV for the undoped case, and 0.73 and 1.03 eV for the n-doped and p-doped cases obtained, respectively, by adding dopant charges $N_d = 3 \times 10^{16}$ cm^{-3} and $N_d = -2 \times 10^{16}$ cm^{-3} in the charge neutrality equation (12).

2.2. SSPC numerical simulation

The energy gap is divided into N trap energy levels E_i ($i = 1, 2, \ldots, N$) with uniform spacing dE. In addition to the free electron and hole densities n and p, the carrier and state densities involved in the steady state quasi-equilibrium at an energy level E_i are the trapped electron

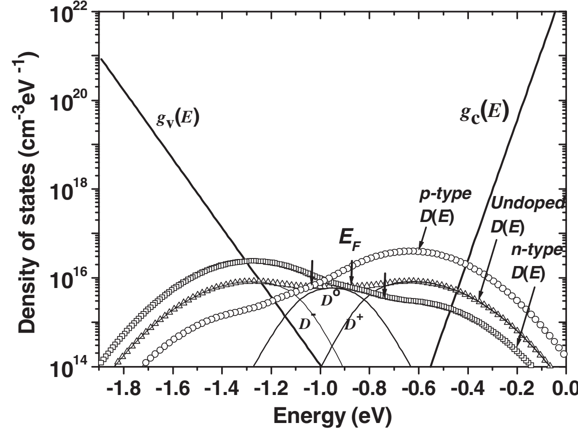

Figure 2. Density of states for undoped ($E_F = -0.87$ eV), n-type ($E_F = -0.73$ eV) and p-type ($E_F = -1.03$ eV) a-Si:H. Also shown are the exponential CBT and VBT state distributions (respectively $g_c(E)$ and $g_v(E)$) and the DB defect state distributions ($D(E)$) calculated by the DPM. The three components D^-, D^0 and D^+ of $D(E)$ for the undoped case are shown in solid lines.

density n_i in the CBT, the trapped hole density p_i in the VBT, the D^- density N_i^-, the D^+ density N_i^+, the total density of CBT/VBT states $N_{ti}^{c/v} = g_{c/v}(E_i)\,dE$ and the total density of DB states $N_{dbi} = D(E_i)\,dE$. The evolution rates of these densities must be equal to zero in the steady state regime, leading to $4N+2$ coupled equations to be solved for $4N+2$ unknown variables: two continuity equations, for n and p,

$$0 = \eta G + \sum_i Re^n_{T,i} + Re^n_{D,i} - \sum_i Rc^n_{T,i} + Rc^n_{D,i} \tag{9}$$

$$0 = \eta G + \sum_i Re^p_{T,i} + Re^p_{D,i} - \sum_i Rc^p_{T,i} + Rc^p_{D,i} \tag{10}$$

and $4N$ equations representing the detailed balance at each trap energy level E_i in the gap for the $4N$ trapped carrier densities n_i, p_i, N_i^+ and N_i^- ($i = 1, 2, \ldots, N$),

$$0 = Rc^n_{T,i} - Re^n_{T,i} + R^n_{hi,i} - R^n_{ho,i}, \tag{11a}$$

$$0 = Rc^n_{D,i} - Re^n_{D,i}, \tag{11b}$$

$$0 = Rc^p_{T,i} - Re^p_{T,i}, \tag{11c}$$

$$0 = Rc^p_{D,i} - Re^p_{D,i}. \tag{11d}$$

The above used rate symbols have the following significance.

$Rc^{n/p}_{T/D,i}$: electron/hole (n/p) capture rate by tail/defect (T/D) states at E_i.
$Re^{n/p}_{T/D,i}$: electron/hole (n/p) emission rate from tail/defect (T/D) states at E_i.
$R^n_{hi,i}$: rate of electron (n) hopping (h) into (i) CBT states at E_i.
$R^n_{ho,i}$: rate of electron (n) hopping (h) out of (o) CBT states at E_i.

The product ηG is the rate of generated electron–hole pairs that have escaped geminate recombination [14]. $G = 10^{20}$ cm^{-3} s^{-1} is the rate of absorption of photons and η the quantum efficiency, assumed to be equal to unity. The solution obtained by solving the $4N+2$ coupled non-linear equations using appropriate numerical methods must satisfy the charge neutrality condition:

$$p + \sum_i p_i + \sum_i N_i^+ - n - \sum_i n_i - \sum_i N_i^- + N_d = 0. \tag{12}$$

The neutral DB density N_i^0 can be found from the DB density conservation equation

$$N_i^0 + N_i^+ + N_i^- = N_{\mathrm{db}i}. \tag{13}$$

The free electron capture and emission rates, $Rc_{T/D,i}^{n/p}$ and $Re_{T/D,i}^{n/p}$, are defined by Simmons and Taylor statistics [7] and have often been used in conventional SSPC simulations that neglect hopping transitions [3, 4, 21]. The additional terms associated with EH transitions in the N equations (11*a*), that concern the trapped electron density n_i into the CBT states, are expressed in terms of the nearest neighbour hopping theory in amorphous semiconductors [22]. According to this approach, the hopping transition occurs via tunnelling between an initial state at the energy level E_i and a neighbouring state at E_j which can be at the same level (iso-energetic hopping), deeper (downward hopping) or shallower (upward hopping). The hopping transport is then based on the single hopping transition rate [22–24]:

$$\Gamma_{i,j} = \nu_{\mathrm{o}}\left(\frac{g_{\mathrm{c}}(E_j)}{G_T}\right) \times \exp\left(-\frac{2R_{i,j}}{a}\right) \qquad \text{if } E_i \geqslant E_j \tag{14a}$$

for iso-energetic and downward hops, with $G_T = \int_{E_{\mathrm{v}}}^{E_i} g_{\mathrm{c}}(E)\,\mathrm{d}E$, the total density of CBT states deeper than E_i, and

$$\Gamma_{i,j} = \nu_{\mathrm{o}}\left(\frac{g_{\mathrm{c}}(E_i)}{G_T}\right) \times \exp\left(-\frac{2R_{i,j}}{a}\right) \times \exp\left(-\frac{E_j - E_i}{k_{\mathrm{B}}T}\right) \qquad \text{if } E_i < E_j \tag{14b}$$

for upward hops, with $G_T = \int_{E_{\mathrm{v}}}^{E_j} g_{\mathrm{c}}(E)\,\mathrm{d}E$ the total density of CBT states deeper than E_j. ν_{o} is the attempt to escape frequency and a is the localization radius of localized states. $g_{\mathrm{c}}(E_j)/G_T$ in equation (14*a*) and $g_{\mathrm{c}}(E_i)/G_T$ in equation (14*b*) are respectively the weighting factors for the hopping probability to a state at $E_j \leqslant E_i$ and to a state at $E_j > E_i$. $R_{i,j}$ is the hopping distance from a state at E_i to a neighbouring state at E_j, given by [25–27]

$$R_{i,j} = \{(4\pi/3)G_T\}^{-1/3} \tag{15}$$

with G_T, as above, having the integral expression depending on whether hopping from E_i is iso-energetic or downward, or it is upward. Having defined the single hopping transition rates $\Gamma_{i,j}$, the above defined total hopping rates out of and into a state at E_i are respectively

$$R_{ho,i}^n = n_i \times \sum_j \Gamma_{i,j} \tag{16a}$$

$$R_{hi,i}^n = \sum_j n_j \times \Gamma_{i,j}. \tag{16b}$$

The energy distribution of the hopping photoconductivity is evaluated by application of the Einstein relation [22]

$$\sigma_{\mathrm{hop}}(E_i) = \frac{e^2}{6kT}(R_{i,j})^2 R_{ho,i}^n \tag{17}$$

and the total hopping photoconductivity is obtained by summation over all the CBT energy levels:

$$\sigma_{\mathrm{hop}} = \frac{e^2}{6kT}\sum_i (R_{i,j})^2 R_{ho,i}^n. \tag{18}$$

The free electron and hole densities in the extended states of the conduction and valence bands contribute to the SSPC following the extended state diffusive photoconductivity

$$\sigma_{\mathrm{ext}} = \mathrm{e}(\mu_n n + \mu_{\mathrm{p}} p) \tag{19}$$

Table 2. Parameters for the SSPC simulation.

$N_c = N_v$ (cm^{-3})	10^{20}
$C_n^o = C_p^o$ (cm^3 s^{-1})	8.5×10^{-8}
$C_n^+ = C_p^-$ (cm^3 s^{-1})	3×10^{-7}
$C_n^c = C_p^v$ (cm^3 s^{-1})	5×10^{-8}
$C_p^c = C_n^v$ (cm^3 s^{-1})	5×10^{-9}
μ_n (cm^2 s^{-1} V^{-1})	10
μ_p (cm^2 s^{-1} V^{-1})	0.3
ν_o (s^{-1})	7×10^{12}
a (cm)	5.12×10^{-8}

where μ_n (μ_p) is the electron (hole) mobility in the conduction (valence) band. With the extended state diffusion and the localized state hopping processes occurring simultaneously, the total SSPC is simply the sum

$$\sigma_{ph} = \sigma_{ext} + \sigma_{hop}. \quad (20)$$

Table 2 lists the parameter values used in our SSPC simulation.

3. Results and discussion

Figure 3 shows the modelled temperature dependence of the normalized SSPC σ_{ph}/eG ($G = 10^{20}$ cm^{-3} s^{-1}), over a temperature range extending from 25 to 500 K, for the undoped case (curve with symbol □), the n-type case (curve with symbol ○) and the p-type case (curves with symbols △ and ◇). It can be seen that the SSPC features described in section 1 (figure 1) are reproduced by the simulation. The simulated SSPC in the thermal quenching region (III) including the local maximum and minimum, shows similar temperature and doping dependence to the measured SSPC (figure 1); on altering the doping smoothly from p-type to n-type, passing the undoped case, this thermal quenching feature shifts towards higher temperature and photoconductivity. Tran [5] studied this feature in detail and concluded that the local maximum and minimum appear in the SSPC when the electron recombination changes path from the VBT states to the DB states, with the latter having higher capture coefficient. The rates

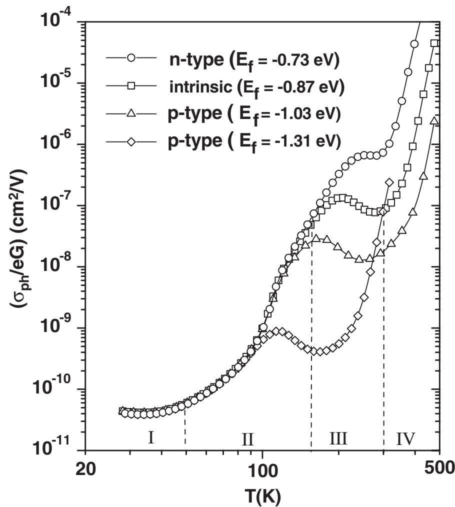

Figure 3. Simulated temperature dependence of the normalized SSPC (σ_{ph}/eG) for undoped a-Si:H and doped a-Si:H at different doping degrees, as indicated by the Fermi-level position in the gap.

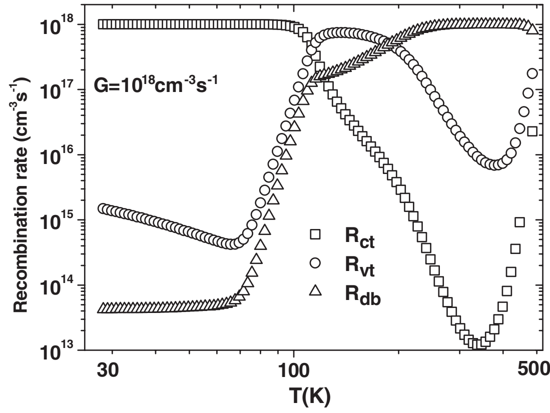

Figure 4. Temperature dependence of the recombination rate via different state species: □ R_{ct}, electron recombination rate via CBT states; ○ R_{vt}, electron recombination rate via VBT states; △ R_{db}, electron recombination rate via DB states.

of electron recombination via CBT, VBT and DB states are plotted as functions of temperature in figure 4 for the undoped case. This shows that the thermal quenching feature (figure 3, undoped curve) occurs effectively around 200 K when recombination changes path from the VBT states (recombination rate R_{ct}) to the DB states (recombination rate R_{db}). Also, in our simulation, the defect density of states model in figure 2 shows that the D^+ and D^0 densities, as electron recombination centres, decrease as the doping is smoothly altered from p- to n-type. This is responsible for the SSPC increase with doping in the thermal quenching region. To reach thermal quenching at higher doping degree, the SSPC requires higher temperature to compensate by increasing the D^+ and D^0 occupation functions (equations (6) and (7)). On the low temperature side, the undoped SSPC in the EH region (I) shows no temperature dependence, $\sigma_{ph}/eG = 4 \times 10^{-11}$ cm^2 V^{-1}, and the onset temperature of this region is about 50 K, in agreement with the data of figure 1.

However, the simulation results show no doping dependence in this region, while the data indicate a SSPC shift down to 10^{-11} cm^2 V^{-1} caused by strong p-type doping. Considering that the electric field acts as an effective temperature in the very low temperature range, Fritzsche *et al* [1] were able to determine, on the basis of experimental results comparing the electric field and temperature dependences of the SSPC, a localization radius for strongly p-type doped a-Si:H corresponding to VBT states. It was then argued that hole hopping photoconduction in the VBT dominates the SSPC at strong p-type doping. One has then to extend the present simulation to include localized–localized state hopping of holes in the VBT, in order to confirm this argument. Although this is not a straightforward task to achieve, complete numerical simulation involving extended and localized states transport of both carrier types is the subject of ongoing work.

Before dealing with the interpretation of the SSPC results, we start by examining the influence of the EH process, as coupled to the other extended–localized state processes (capture, emission, generation and recombination). Figure 5 shows the energy distribution of the trapped electron density n_i in the CBT for selected temperature values from 30 to 110 K, in the EH dominated range (see sections below). A demarcation energy level E_d^{hop} associated with the peak of the distribution shifts up to shallower states and increases in magnitude as the temperature decreases (indicated by arrows), while the distribution width above the peak decreases away from the CB. From 50 K down, the peak stops shifting near the energy -0.2 eV and the distribution remains almost unaltered, resulting in a narrow temperature independent band. This is clarified in figure 6, where this demarcation energy is plotted as a function of temperature (+ symbol). The demarcation energy E_d^{ext}, defined in the same way but using

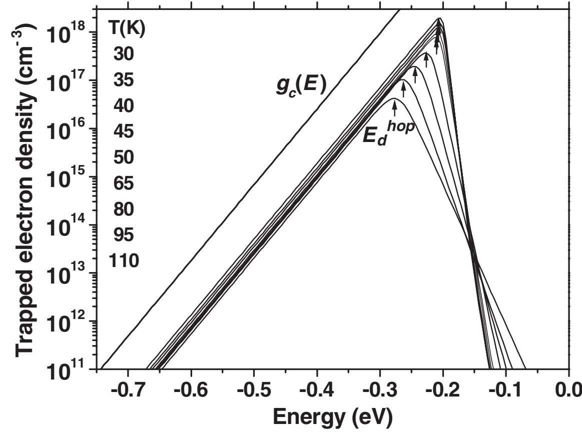

Figure 5. Energy distribution of the trapped electron density n_i at several temperatures between 30 and 110 K (in the EH dominated range). The temperatures are ordered in the inset column so that the demarcation energy $E_{\mathrm{d}}^{\mathrm{hop}}$ defined by the distribution peak shifts towards the CB as the temperature decreases. As indicated by the arrows, $E_{\mathrm{d}}^{\mathrm{hop}}$ stops shifting around −0.2 eV for the last five temperature values from 50 K down.

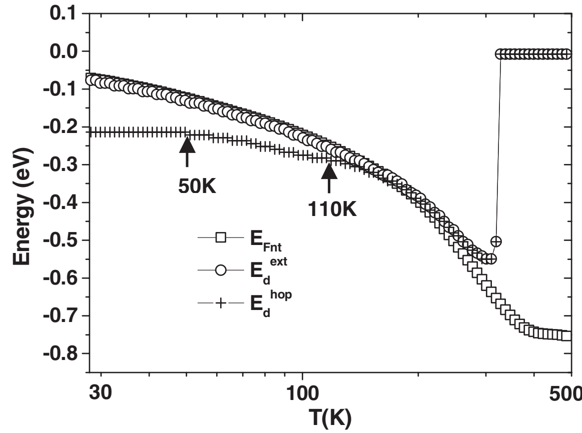

Figure 6. Temperature dependence of the demarcation energy $E_{\mathrm{d}}^{\mathrm{hop}}$ identified by the trapped electron distribution peak (figure 5), as compared to the trapped electron quasi-Fermi level defined by Simmons and Taylor (equation (21)). The demarcation energy $E_{\mathrm{d}}^{\mathrm{ext}}$ defined in the same way, but using conventional simulation based on extended state conduction (i.e. without EH), is also shown for comparison.

conventional simulation based on extended state conduction (without considering EH), is shown for comparison (○ symbol). The trapped electron quasi-Fermi level E_{Fnt} defined by Simmons and Taylor [7] is also plotted against temperature as a reference for $E_{\mathrm{d}}^{\mathrm{hop}}$ and $E_{\mathrm{d}}^{\mathrm{ext}}$ (□ symbol):

$$E_{\mathrm{Fnt}} = E_{\mathrm{c}} + k_{\mathrm{B}}T \ln\left(\frac{C_n^c n + C_{\mathrm{p}}^c p}{C_n^c N_{\mathrm{c}}}\right). \tag{21}$$

Before comparison with the Simmons and Taylor statistics, we should exclude first the region

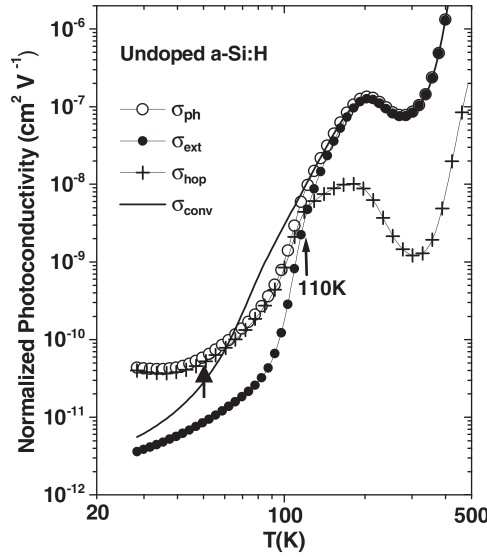

Figure 7. The extended state photoconductivity σ_{ext} (● symbol) and the EH photoconductivity σ_{hop} (+ symbol) components of the SSPC σ_{ph} (○ symbol). The conventional SSPC σ_{Conv} (solid line) simulated without EH consideration is also shown for comparison.

above about 250 K dominated by divalent DB state statistics (figure 4). Below 250 K, where recombination is controlled by monovalent band tail states (figure 4), E_d^{ext} does evidently superimpose E_{Fnt} since Simmons and Taylor statistics, with only extended–localized state transitions, is applied. In the presence of EH, the demarcation energy E_d^{hop} deviates left below E_{Fnt} at about 110 K, thus defining a new mean trapped electron quasi-Fermi level, representative of all combined extended–localized and localized–localized carrier transitions. Comparing E_d^{hop} with E_d^{ext}, we remark that they fit each other above 110 K and one can then identify a transition temperature, around 110 K (arrow indication), between the region of high temperature extended state photoconduction and the region of low temperature localized state hopping photoconduction. There is also another transition temperature at about 50 K (arrow indication), below which the new quasi-Fermi level E_d^{hop} stops shifting upward and stays close to -0.2 eV. This is consistent with the photoconductivity behaviour with temperature, as will be discussed below.

To illustrate the relative contribution of EH to the SSPC as a function of temperature, we plot in figure 7 the normalized SSPC σ_{Ph}/eG (curve with symbol ○) and conventional SSPC σ_{Conv}/eG obtained without EH consideration (curve with solid line). σ_{Conv} is a result of an SSPC simulation performed without the hopping terms in the rate equation (11*a*) and is given by an equation similar to equation (19). We also show the two SSPC components due to extended state conduction (σ_{ext}/eG with symbol ●) and localized states EH (σ_{hop}/eG with symbol +) to examine the relative contribution of each. The comparison is made for undoped a-Si:H with $G = 10^{20}$ cm^{-3} s^{-1}. On decreasing the temperature, the EH process starts having an effect at about 110 K and becomes gradually more pronounced as the temperature decreases. The total SSPC can be approximated by the EH photoconductivity ($\sigma_{ph} \sim \sigma_{hop}$) over the whole temperature range below 110 K. Hence, the inclusion of EH clearly brings in the necessary correction to conventional SSPC simulation based exclusively on extended states conduction [3, 4, 21]. The onset temperature 110 K of the EH photoconductivity in figure 7 is

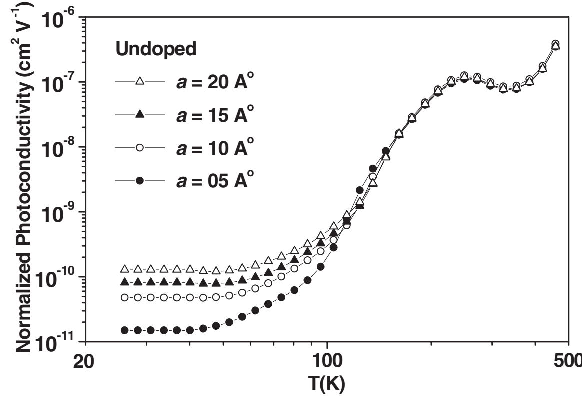

Figure 8. Temperature dependence of the normalized SSPC for the undoped case at four different values of the localization radius a, indicating the sensitivity of the SSPC low temperature region (I) to this parameter: $a = 5$ Å (symbol ●), $a = 10$ Å (symbol ○), $a = 15$ Å (symbol ▲), and $a = 20$ Å (symbol △).

consistent with the appearance of the demarcation energy E_d^{hop} as an alternative trapped electron quasi-Fermi level in figure 6. Decreasing the temperature further causes the SSPC to level out at about 50 K and show the low temperature normalized SSPC of 4×10^{-11} cm^2 V^{-1}. We note here that the transition temperature around 50 K, below which the hopping photoconductivity levels out, is the same transition temperature below which the quasi-Fermi level E_d^{hop} stops shifting upward (figure 6) and the trapped electron density distribution remains without alteration (figure 5). Shklovskii *et al* [14] developed a theory to explain the SSPC in region (I), according to which EH is defined by the probability for electrons to escape the geminate recombination. The SSPC is then due to field extraction of electrons that have reached a distance from their own holes corresponding to equal rates of geminate recombination and EH. The theoretical expression of σ_{ph}/eG is

$$\frac{\sigma_{Ph}}{eG} = \frac{ea^2}{12kT_c} \ln(\nu_0\tau_0)L \tag{22}$$

L (in units of a) represents the normalized average photocarrier separation and τ_0 the geminate recombination time. For assumed $a = 10^{-7}$ cm, $\nu_0\tau_0 = 10^4$, $kT_c = 0.025$ eV and $G = 10^{20}$ cm^{-3} s^{-1}, L is about 15 and $\sigma_{Ph}/eG = 5 \times 10^{-12}$ cm^2 V^{-1}.

Comparing to our simulation results, one has to note that the effect of the quantum efficiency η is included in the derivation of σ_{ph} in the Shklovskii model, while it is neglected in the simulation ($\eta = 1$). Referring to equation (18) and equation (22) expressing the SSPC for the present simulation and the model of Shklovskii respectively, it appears that three common parameters (a, ν_0 and kT_c) control the level of the SSPC in region (I) and that this is most sensitive to the localization radius a. In figure 8, we present for the undoped case the temperature dependence of σ_{ph}/eG at four different values of a, with the other parameters $kT_c = 0.025$ eV and $\nu_0 = 10^{12}$ s^{-1} as in the Shklovskii model. Clearly figure 8 confirms the sensitivity of region (I) of the SSPC to a, and for the same value $a = 10$ Å as in the Shklovskii model $\sigma_{ph}/eG \sim 4.8 \times 10^{-11}$ cm^2 V^{-1} is about one order of magnitude higher than that of Shklovskii. This can be due to one order of magnitude drop, at low temperature, of the quantum efficiency η [12] that is not considered in the simulation. With the quantum efficiency effect taken into account, the parameters can be adjusted within reasonable ranges to agree with the experimental SSPC in region (I).

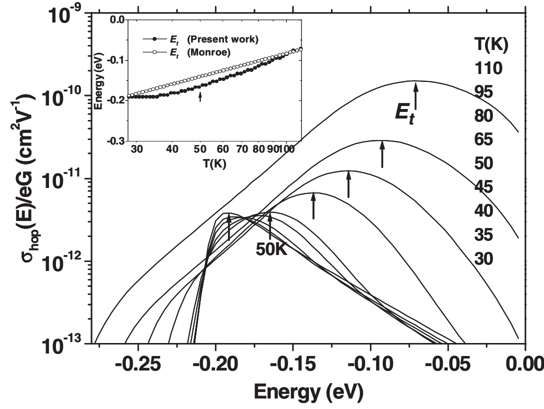

Figure 9. Energy distribution of the EH photoconductivity $\sigma_{\mathrm{hop}}(E)$ at several temperatures between 30 and 110 K (in the EH dominated range). The temperatures are ordered in the inset column so that transport energy E_{t} associated with the distribution peak shifts towards the CB as the temperature increases. The inset figure indicates the temperature dependence of the simulated E_{t} (symbol ●) as compared to Monroe [16] definition of E_{t} (symbol ○).

Figure 9 shows the energy distribution of the EH photoconductivity $\sigma_{\mathrm{ph}}(E)$ given by equation (17) for several temperatures between 30 and 110 K (in the EH dominated range). A conduction path is illustrated around the peak of each distribution and the energy level at the distribution peak can be termed, after Monroe, transport energy E_{t} [15, 16]. This shifts to deeper states with decreasing temperature. Figure 9 also shows that the distribution $\sigma_{\mathrm{ph}}(E)$ remains with no appreciable alteration for the temperature values below 50 K. The temperature dependence of E_{t} is shown in the inset figure and one can see that E_{t} stays at an average position near -0.2 eV below 50 K, as the distribution $\sigma_{\mathrm{ph}}(E)$ stops shifting further. This clearly explains the constant normalized SSPC $\sigma_{\mathrm{ph}}/eG \sim \sigma_{\mathrm{hop}}/eG \sim 4 \times 10^{-11}$ cm^2 V^{-1} below 50 K, which is nothing but the integrated area of $\sigma_{\mathrm{ph}}(E)$. The inset figure shows also, for comparison, the temperature dependence of E_{t} as given by Monroe:

$$E_{\mathrm{t}} = kT_{\mathrm{c}} \ln\left(\frac{8}{27a^3kT_{\mathrm{c}}G_{\mathrm{c}}}\right) - 3T_{\mathrm{c}} \ln\left(\frac{T_{\mathrm{c}}}{T}\right). \qquad (23)$$

Although the two curves follow different temperature variations, the maximum difference of about 0.03 eV between the two data sets could account for the different photo-response to the transient photo-excitation considered in the model of Monroe.

In figure 10, we further decompose the SSPC in the undoped case to reveal the details of the electron and hole photoconductivity behaviours with temperature. The SSPC above 110 K is due to extended state photoconductivity σ_{ext} and this is mainly controlled by electrons ($\sigma_{\mathrm{ext}} \sim e\mu_n n$). As the temperature decreases below 110 K, the EH becomes gradually dominant and the SSPC smoothly switches to hopping dominated photoconductivity σ_{hop}. The extended state photoconductivity, still dominated by electrons ($\sigma_{\mathrm{ext}} \sim e\mu_n n$), decreases rapidly until about 90 K. Below 90 K, the hole extended state photoconductivity becomes dominant ($\sigma_{\mathrm{ext}} \sim e\mu_n p$), whereas the electron extended state photoconductivity $e\mu_n n$ continues decreasing steadily until about 70 K. From 70 K down, this reaches a very low temperature independent value, $e\mu_n n/(eG) \sim 2 \times 10^{-13}$ cm^2 V^{-1}. Referring to figure 4, the temperature region below 70 K falls within the limits where the electron recombination is controlled by the CBT states with constant rate $R_{\mathrm{ct}} \sim G$. It is then concluded that 70 K is a transition temperature below which the electrons undergo a monomolecular recombination

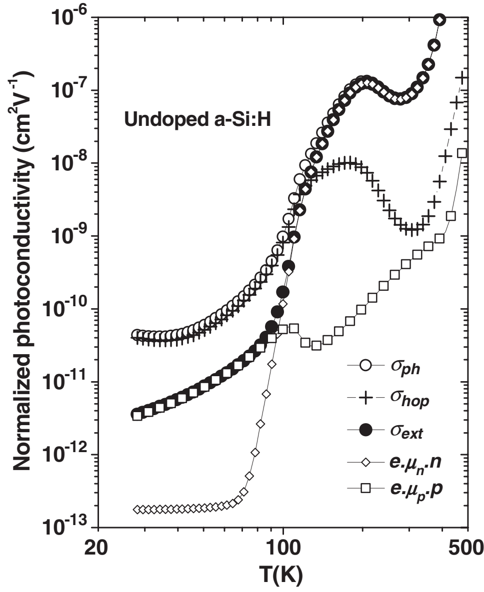

Figure 10. Decomposition of the SSPC $\sigma_{\rm ph}$ (symbol ○) into localized state EH photoconductivity $\sigma_{\rm hop}$ (symbol +), extended state electron photoconductivity $e\mu_n n$ (symbol ◇) and extended state hole photoconductivity $e\mu_{\rm p} p$ (symbol □), for the undoped case.

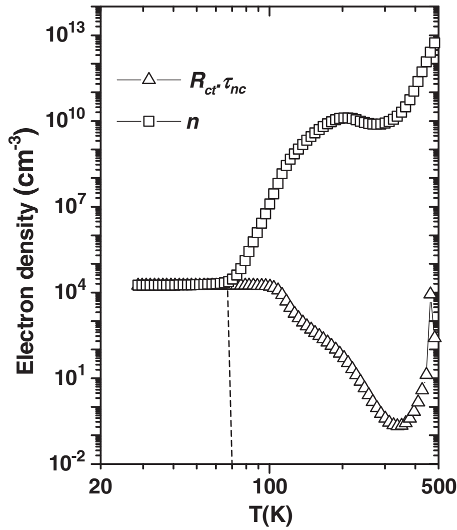

Figure 11. Temperature dependence of the free electron density n (symbol □), as compared to the product of the recombination rate via CBT states $R_{\rm ct}$ and the corresponding lifetime $\tau_{\rm nc} = [C_n^c \sum_i (N_{\rm ti} - n_i)]^{-1}$ (symbol Δ). From 70 K down, $n = R_{\rm ct}\tau_{\rm nc}$, indicating a monomolecular recombination to CBT states.

to CBT states, with $\tau_{\rm nc} = [C_n^c \sum_i (N_{\rm ti} - n_i)]^{-1}$ the corresponding lifetime. Figure 11 shows the temperature dependence of the free electron density n (symbol □) and the product $\tau_{\rm nc} R_{\rm ct}$ (symbol Δ). The relation $n = \tau_{\rm nc} R_{\rm ct}$ expressing monomolecular recombination to CBT states is confirmed below 70 K (vertical dashed line). Note that this carrier behaviour follows the present simulation, which neglects the localized state hopping of holes, and that if hole hopping through the VBT states were included the extended state photoconductivity $\sigma_{\rm ext}$ could be controlled by electrons in this low temperature region. However, the total SSPC $\sigma_{\rm ph}$ that should be compared to experimental SSPC is not influenced by this detail. This is dominated by the EH component $\sigma_{\rm hop}$ over the entire temperature range below 110 K.

4. Conclusion

The temperature dependence of SSPC in a-Si:H, in the range from 25 to 500 K, is studied in terms of a model coupling the extended state free carrier transport and the localized state electron hopping transport. The results are compared to those obtained by conventional simulations that ignore localized–localized state transitions. A smooth transition around 110 K separates the high temperature extended state transport and the low temperature localized state hopping transport. The observed constant normalized SSPC $\sigma_{Ph}/eG \sim 4 \times 10^{-11}$ cm^2 V^{-1} in the temperature range below 50 K is reconfirmed. This is consistent with the temperature change in the energy distribution of the hopping photoconductivity, that shows no appreciable variation below 50 K. Also, the DPM adopted for the DB defect density of states proves compatible with the simulation model and provides a reasonable explanation of the doping effect on the SSPC temperature dependence. The experimental observation that p-type doping can considerably lower the SSPC in the low temperature hopping region is not reproduced by the present simulations and would appear to require inclusion of hole hopping in the VBT.

Acknowledgment

We are grateful to Professor H Fritzsche for provision of SSPC data.

References

[1] Fritzsche H *et al* 1992 Some observations on the photoconductivity of amorphous semiconductors *J. Non-Cryst. Solids* **141** 123 (reprinted with permission from Elsevier)
[2] Vomvas A and Fritzsche H 1987 *J. Non-Cryst. Solids* **97/98** 823
[3] Vaillant F, Jousse D and Bruyere J-D 1988 *Phil. Mag.* B **57** 649
[4] Smail T and Mohammed-Brahim T 1991 *Phil. Mag.* B **64** 675
[5] Tran M Q 1995 *Phil. Mag.* B **72** 35
[6] Cleve B and Thomas P 1990 *Proc. MRS Spring Mtg (San Francisco, 1990)*
[7] Simmons J G and Taylor G W 1971 *Phys. Rev.* B **4** 502
[8] Dersch H, Schweitzer L and Stuke J 1983 *Phys. Rev.* B **28** 4678
[9] Zhou J H and Elliot S R 1992 *Phil. Mag.* B **66** 801
[10] Zhou J H and Elliott S R 1993 *Phys. Rev.* B **48** 1505
[11] Cloude C, Spear W E, LeComber P G and Hourd A C 1986 *Phil. Mag.* B **54** L113
[12] Spear W E and Cloude S C 1988 *Phil. Mag.* B **58** 467
[13] Johanson R E 1992 *Phys. Rev.* B **45** 4089
[14] Shklovskii B I, Fritzsche H and Baranovskii S D 1989 *Phys. Rev. Lett.* **62** 2989
[15] Monroe D 1985 *Phys. Rev. Lett.* **54** 146
[16] Baranovskii S D, Thomas P and Adriaenssens G J 1995 *J. Non-Cryst. Solids* **190** 283
[17] Powell M J and Deane S C 1993 *Phys. Rev.* B **48** 10815
[18] Powell M J and Deane S C 1996 *Phys. Rev.* B **33** 10121
[19] Main C, Marshall J M and Reynolds S 2005 *J. Optoelectron. Adv. Mater.* **7** 107
[20] Okamoto H, Kida H and Hamakawa Y 1984 *Phil. Mag.* B **49** 231
[21] Main C, Berkin J and Merazga A 1991 *New Physical Problems in Electronic Materials* ed M Borissov *et al* (Singapore: World Scientific) pp 55–86
[22] Mott N F and Davis E A 1979 *Electronic Processes in Non-crystalline Materials* (Oxford: Clarendon)
[23] Miller A and Abrahams E 1960 *Phys. Rev.* **120** 745
[24] Godet C 2001 *Phil. Mag.* B **81** 205
[25] Baranovskii S D, Rubel O and Thomas P 2005 *Thin Solid Films* **487** 2–7
[26] Marshall J 2000 *Phil. Mag. Lett.* **80** 691
[27] Marshall J 2003 *J. Mater. Sci., Mater. Electron.* **14** 611